Theory of laser-induced ultrafast superdiffusive spin transport in layered heterostructures

M. Battiato,* K. Carva,† and P. M. Oppeneer
Department of Physics and Astronomy, Uppsala University, Box 516, SE-75120 Uppsala, Sweden
(Received 2 April 2012; published 5 July 2012)

Femtosecond laser excitation of a ferromagnetic material creates energetic spin-polarized electrons that have anomalous transport characteristics. We develop a semiclassical theory that is specifically dedicated to capture the transport of laser-excited nonequilibrium (NEQ) electrons. The randomly occurring multiple electronic collisions, which give rise to electron thermalization, are treated exactly and we include the generation of electron cascades due to inelastic electron-electron scatterings. The developed theory can, moreover, treat the presence of several different layers in the laser-irradiated material. The derived spin-dependent transport equation is solved numerically and it is shown that the hot NEQ electron spin transport occurs neither in the diffusive nor ballistic regime, it is superdiffusive. As the excited spin majority and minority electrons in typical transition-metal ferromagnets (e.g., Fe, Ni) have distinct, energy-dependent lifetimes, fast spin dynamics in the femtosecond (fs) regime is generated, causing effectively a spin current. As examples, we solve the resulting spin dynamics numerically for typical heterostructures, specifically, a ferromagnetic/nonmagnetic metallic layered junction (i.e., Fe/Al and Ni/Al) and a ferromagnetic/nonmagnetic insulator junction (Fe or Ni layer on a large band-gap insulator as, e.g., MgO). For the ferromagnetic/nonmagnetic metallic junction where the ferromagnetic layer is laser-excited, the computed spin dynamics shows that injection of a superdiffusive spin current in the nonmagnetic layer (Al) is achieved. The injected spin current consists of screened NEQ, mobile majority-spin electrons and is nearly 90% spin-polarized for Ni and about 65% for Fe. Concomitantly, a fast demagnetization of the ferromagnetic polarization in the femtosecond regime is driven. The analogy of the generated spin current to a superdiffusive spin Seebeck effect is surveyed.

DOI: 10.1103/PhysRevB.86.024404 PACS number(s): 75.78.Jp, 72.25.−b, 75.76.+j, 72.10.Bg

I. INTRODUCTION

Advances in the generation of ultrashort laser pulses led to the development of the femtosecond pump-probe technique in the eighties,[1–3] which has initiated a viable approach to study carrier dynamics on a time scale previously inaccessible. The novel experimental tool led to new discoveries, such as that of unusual fast dynamics of laser-excited nonequilibrium (NEQ) electrons in metal films.[4–7] It also gave rise to new theoretical challenges and opportunities. A considerable theoretical effort has meanwhile been undertaken[8–15] with the aim to provide a working model for the dynamics of NEQ electrons induced by a femtosecond laser excitation. Unfortunately, still not everything is understood regarding the ultrafast motion of hot NEQ electrons.

An interesting research field that, too, has become unlocked through the above advancement is that of the ultrafast laser-induced manipulation of magnetic order on the femtosecond time scale (see, e.g., Ref. 16 for a recent review). It was originally discovered by Beaurepaire *et al.*[17] that a femtosecond laser pulse could quench the ferromagnetic order in Ni on an unprecedented time scale of 200–300 fs. Before this discovery, such ultrafast magnetization quenching was considered to be unachievable (see, e.g., Ref. 18). Since then, the microscopic origin of ultrafast laser-induced demagnetization has become a hotly debated topic.[19–35] As the spin angular momentum is a conserved quantity, it has frequently been proposed that there must exist some ultrafast dissipation channel for spin angular momentum. Possible channels that have been proposed are, e.g., the Elliott-Yafet electron-phonon spin-flip scattering,[19,30,34] electron-magnon[36] or electron-electron scattering,[23] or relativistic laser-field induced spin-flips.[24] A viable modeling approach appears nonetheless to assume a spin-relaxation time due to an unspecified microscopic mechanism and perform equilibrium atomistic simulations of the laser-induced magnetization dynamics.[37–42]

In a previous paper,[29] we have pointed out that there exists a considerable interplay of the phenomena of ultrafast demagnetization and of femtosecond spin transport by showing that spin-dependent electron transport in the superdiffusive regime is, in principle, able to explain completely the ultrafast demagnetization without recurring to the still controversial channels of dissipation of angular momentum.[25,30,31,33,35] Moreover, we have shown how the existence of ultrafast demagnetization only in metals (in dielectrics and half-metals it is orders of magnitude slower[16,43]) and the saturation of the demagnetization[16] follow naturally from the description of spin-dependent NEQ electron transport. In the aforementioned paper,[29] we predicted that femtosecond laser-excitation of the ferromagnetic material would lead to demagnetization of the ferromagnet as well as the occurrence of an ultrafast spin current (which carries away spin angular momentum).

While we believe that our predictions will soon be validated by experimental findings, it deserves to be mentioned that several recent papers have appeared that presented arguments *against* a notable influence of superdiffusive spin transport.[33,44,45] A first indication of the existence of laser-induced spin-transport has been reported recently,[32] and our findings are not incompatible with an earlier work,[22] but these are definitely far from being conclusive evidences. Hence, it is, to date, not yet possible to conclude to what extent NEQ superdiffusive spin transport contributes to the demagnetization and even less to rule out whether it is its only driver or just a side actor.

The purpose of the present paper is to make a step forward in the theoretical description of ultrafast demagnetization and electronic spin transport on the femtosecond time scale and elucidate further their interconnections. Several different approaches[5,9–12,14,15] have been attempted before to model the femtosecond electron motion, but these always rely heavily on approximations. The two limits of transport, standard diffusion (Brownian motion) and ballistic transport have been used previously, as well as mixtures of the two. However, both the standard diffusion and the ballistic diffusion models fail to capture the regime of energetic electronic transport.[4] In metals, electron lifetimes are of the order of few tens of femtoseconds and the mean free paths up to tens of nanometers. These values are absolutely comparable with the time scale under analysis and the length scale involved (for instance, the penetration depths of optical lasers in metals is within a few tens of nanometers). Assuming that the particle mean-free path is almost zero $\lambda \to 0$ and its velocity almost infinity $v \to \infty$, as assumed for the standard diffusion, will lead to unacceptable errors. Similarly, simplistic ballistic transport cannot describe the diffusive-like behavior of the electrons, undergoing several scattering events.[4] Mixing the two regimes within one formalism[11] provides a more powerful fitting procedure but does not answer to the need of a proper description of NEQ electron motion over a wide range of time and length scales.

Moreover, in previous approaches often the definition of a local electron temperature is used.[10–12,15] However, it is known that the electron system in metals is in a strongly out-of-equilibrium state up to several hundreds of femtoseconds after the laser excitation.[46–49] Besides, the states well above the Fermi energy are the ones that mostly contribute to the femtosecond transport. For this reason, a model aiming to have predictive power on the femtosecond time scale cannot rely on the assumption of an instantaneous electron temperature. In principle, the Boltzmann equation for both the energy and the position is to be solved. But, as for instance in Ref. 9, the numerical cost forced the authors to over approximate the description of the material. We will start from a similar theoretical background, but we will integrate analytically the geometry of the motion leading to a far less expensive description. This will allow us to abandon most approximations: the relaxation-time approximation of the Boltzmann transport equation, the close to thermal equilibrium assumption, or any simplified description of the material. Energy- and spin-dependent lifetimes and velocities will be used, including in this way the real band structure of the material. Henceforth, the here-developed model has no fitting parameters. In addition, as inelastic electron-electron scatterings and electron cascades are included, the effects of electron thermalization are fully incorporated. The developed model is thus specifically derived to describe the electron dynamics in strongly out-of-equilibrium conditions within the subpicosecond time domain, and evolving towards equilibration.

In the following, we present a rigorous derivation for laser-induced NEQ electron dynamics in layered materials and heterostructures. The treated process is schematically shown in Fig. 1. We analytically derive the governing spin- and energy-dependent transport equation, whose time dependence is numerically solved. We explicitly study the laser-induced spin and electron dynamics in four typical heterostructures, viz., the ferromagnetic/nonmagnetic metal junctions Fe/Al and Ni/Al, and the ferromagnetic metal/nonmagnetic insulator junctions Fe/MgO and Ni/MgO. Due to distinct energy-dependent lifetimes of the laser-excited electrons in the ferromagnet, effectively, an ultrafast flow of spin-polarized electrons is induced, which leads to injection of a highly polarized (up to 90% for Ni) spin current in the nonmagnetic metallic layer. The significance of the creation of the spin current is worked out further, as it may open a new way to utilize chargeless spin transport as a means to transport information on the femtosecond time scale (cf. Refs. 50–53). We also point out the analogy between the laser-generated spin current and that occurring through the spin Seebeck effect.[54–57]

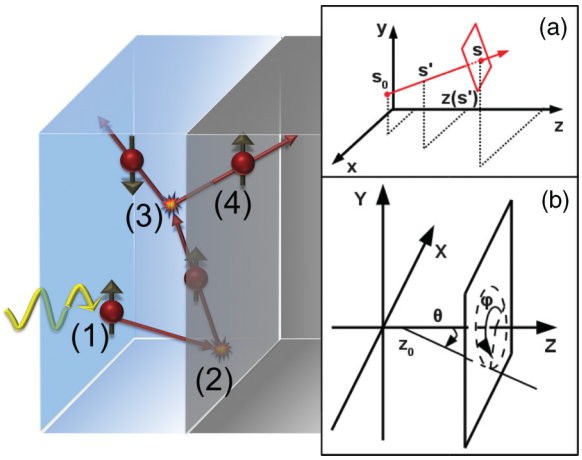

FIG. 1. (Color online) Sketch of the laser-induced electronic motion on the femtosecond timescale. After the laser excitation (1) the hot NEQ electron starts its motion in a random direction. It travels on a straight trajectory until it suffers a scattering (2) and is bounced back in any random direction. The electron can also undergo an inelastic scattering (3) where another electron is ousted from bands below the Fermi energy. While traveling the electron can eventually cross the interface between two materials (4). (a) shows the geometry for Eqs. (1) and (2) and for the calculation of the quasi 1D integrated flux φ^{1D} in Eq. (3). (b) depicts the geometry to compute the integrated flux φ^{3D} in Eq. (6).

II. INTRODUCTION TO THE MODELED SYSTEMS AND APPROXIMATIONS

Our first aim is to give a geometrically exact description of the kinematics of excited NEQ electrons. Since the derivation in Sec. III is lengthy and not always straightforward, we provide in this section a purely descriptive explanation of the underlying physics, which will be exactly modeled mathematically in the subsequent sections.

We will describe the motion of an electron excited by some means (usually by a photon) to a given energy [see Fig. 1 stage (1)]. We assume the probability distribution of the final energy (and of the final spin state) to be known, for instance from *ab initio* calculations.[58] Simultaneously a hole will be created in the valence band. The same kinematic treatment applies to holes as well but, as argued below, often their mobility is

negligible on the considered timescale and for this reason their transport will be neglected in the following.

After the first excitation, the energetic electron will start traveling. We assume the possible emission direction to be isotropically distributed over all solid angles and that the electron dispersion $E = E(\mathbf{k})$ is simply $E = E(|\mathbf{k}|)$. This is not strictly true but except for highly anisotropic crystals this is indeed a very good approximation. Also, the only external source of linear momentum that would, in principle, be able to give a preferential direction to the motion after the excitation is the photon itself but since it carries an extremely small linear momentum this can be safely neglected.[59,60]

The trajectory until the first scattering event [see Fig. 1 stage (2)] will be considered a straight line, traversed with a velocity dependent only on the energy of the traveling electron and the material. In this assumption, two effects are neglected: external fields and refraction at interfaces. Regarding external fields, only extremely large ones can give significant contributions to the transport on the femtosecond timescale. For commonly sized electric or magnetic fields a slower drift of the center of motion will be occurring on longer timescales, but we are not interested in those at the moment. Nonetheless, one might argue that in highly excited situations the electronic diffusion itself creates internal fields by leading to an imbalance of charge. In reality, these fields are never present because they are screened out very quickly and efficiently[61] (we will come back to this assumption in Sec. V A). Neglecting the second effect, the interface reflection, leads instead to a more delicate approximation. In case an electron crosses the interface between two materials [see Fig. 1 stage (4)], we assume that the direction of the velocity in the second medium will be the same as in the first one, while the modulus will be given by the dispersion relation $E = E(|\mathbf{k}|)$ in the second material. This choice does preserve the energy but not the crystal momentum. This delicate conservation law can be restored approximately by treating the surface between two materials as a partially reflecting surface but we will not treat this effect in the following.

While the electron traverses the trajectory, it has a certain probability per unit time to be scattered. Upon scattering it changes the direction of its motion and may eventually loose part of its energy. If it scatters with a phonon or an impurity, the scattering can be considered with a very good approximation as elastic [see Fig. 1 stage (2)]: the energy is almost not changed and the momentum is randomized with almost no correlation with the incoming direction. If the excited electron scatters with other electrons at or below the Fermi energy, the scattering is inelastic and its energy is going to be changed [see Fig. 1 stage (3)]. We again assume that the transition probability to different final energies is a known function. Unfortunately, the outgoing direction in this case is correlated to the incoming one. Even so, in the materials of our interest such as Ni the larger effective mass of d electrons at the Fermi energy compared to the traveling sp-like electron encourages the use of the same approximation. After the scattering, the electron will move as already described but with eventually a different energy.

We also take into account that an electron undergoing an inelastic scattering may loose sufficient energy that it can excite a second electron to above the Fermi energy [see Fig. 1 stage (3)]. Again, the direction of the motion of this cascade electron is correlated to the incoming and outgoing direction of the exciting electron. We, however, neglect this and assume again an isotropic distribution of possible emission directions. We stress that both, this and the previous, approximation on the emission direction will lead to an underestimation of the diffusion process.

III. DERIVATION OF THE KINEMATIC MODEL

We develop here an uniaxial model, where only the z dependence—being normal to the layers—is kept because we are interested in relatively thin film junctions where only the spatial inhomogeneity (due to the appearance of several films) is important along the z direction. Nonetheless, the same approach can be used to describe systems with lower symmetry as well as lateral spin transport in quasi-two-dimensional structures. In the following, majority- and minority-spin electrons will be described by the same mathematical model but with different values of the parameters.

As the derivation involves many variables, in the following we show only those that are relevant at that moment of the derivation. Also, we will label as belonging to the first generation those electrons that have been excited by the laser before they experience the first scattering event. Electrons coming out of the first scattering until the second one will be referred to as second generation electrons and so on.

A. Equation of motion of a particle

We start with computing some introductory quantities. Assuming a given emission direction the equation of motion $s(t)$ of a first-generation electron in terms of the coordinate on the trajectory s [see, in Fig. 1(a)] is

$$\int_{s_0}^{s(t)} \frac{ds'}{v(z(s'))} = t - t_0 \,, \tag{1}$$

where $t - t_0$ is the time needed to reach $s(t)$ starting the motion in s_0 and $v(\sigma, E, z)$ is the velocity, $z(s)$ is the z projection of the position corresponding to the coordinate on the trajectory s and σ and E represent respectively the spin and the energy of the considered electron. It is not possible to have an explicit form of $s(t)$ because the velocity is position dependent. The probability to reach a point s without being scattered obeys

$$P(s) = \exp\left[-\int_{s_0}^{s} \frac{ds'}{\tau(s')v(s')}\right], \tag{2}$$

where $\tau(\sigma, E, z)$ is the electron lifetime (i.e., average time before the electron is scattered), with $P(0) = 1$ and $P(+\infty) \to 0$.

B. From the flux of the 1D case . . .

Using Eqs. (1) and (2), we can compute the integrated flux φ^{1D}, that is the average fraction of a first-generation electron that has crossed a point s before time t, given it was emitted

in s_0 at time t_0 [see, Fig. 1(a)],

$$\varphi^{1D}(s,t) = \exp\left[-\int_{s_0}^{s}\frac{ds'}{\tau(s')v(s')}\right]\Theta\left[t-t_0-\int_{s_0}^{s}\frac{ds'}{v(s')}\right]\Theta[t-t_0]. \tag{3}$$

The step function $\Theta[t-t_0]$ is due to the fact that before t_0 the electron was not excited and therefore no contribution is present. The other step function allows a contribution only if there was enough time for the electron to reach the point s. The exponential represents the fact that if the electron is scattered it does not contribute anymore to φ^{1D}.

C. . . . to the 3D case

We are now able to compute the statistically averaged integrated flux φ^{3D} through a surface normal to the z axis and located in z given by a first-generation electron emitted in a random direction [see, Fig. 1(b)]. Having assumed the emission direction probability to be isotropic on all solid angles, the integrated flux φ^{3D} is given by (with the integration over the spherical coordinate ϕ already computed)

$$\varphi^{3D}(z,t) = \int_0^{\frac{\pi}{2}}\frac{\sin\theta}{2}\exp\left[-\int_{\frac{z_0}{\cos\theta}}^{\frac{z}{\cos\theta}}\frac{dz'}{\tau(z'\cos\theta)v(z'\cos\theta)}\right]\Theta\left[t-t_0-\int_{\frac{z_0}{\cos\theta}}^{\frac{z}{\cos\theta}}\frac{dz'}{v(z'\cos\theta)}\right]\Theta[t-t_0]\,d\theta. \tag{4}$$

This expression can be simplified to

$$\varphi^{3D}(z,t) = \int_0^{\frac{\pi}{2}}\frac{\sin\theta}{2}\exp\left[-\frac{1}{\cos\theta}\int_{z_0}^{z}\frac{dz''}{\tau(z'')v(z'')}\right]\Theta\left[t-t_0-\frac{1}{\cos\theta}\int_{z_0}^{z}\frac{dz''}{v(z'')}\right]\Theta[t-t_0]\,d\theta \tag{5}$$

and finally to

$$\varphi^{3D}(z,t) = \int_0^{\arccos\left(\frac{1}{t-t_0}\int_{z_0}^{z}\frac{dz'}{v(z')}\right)}\frac{\sin\theta}{2}\times\exp\left[-\frac{1}{\cos\theta}\int_{z_0}^{z}\frac{dz'}{\tau(z')v(z')}\right]\Theta[t-t_0]\,d\theta. \tag{6}$$

Being interested only in the flux $\phi_\delta = \partial\varphi^{3D}/\partial t$, we have to differentiate Eq. (6) with respect to time. The differentiation is long and tedious, but straightforward. We report only the final result, which is surprisingly simple:

$$\phi_\delta(z,t|z_0,t_0) = \frac{\partial}{\partial t}\varphi^{3D}(z,t) = \frac{[\widetilde{\Delta t}]}{2(t-t_0)^2}\times\exp\left[-(t-t_0)\left[\frac{\widetilde{\Delta t}}{\tau}\right][\widetilde{\Delta t}]^{-1}\right]\Theta\left[t-t_0-|[\widetilde{\Delta t}]|\right]. \tag{7}$$

Note that we suppressed the no-longer-useful superscript "3D," wrote explicitly the dependence on the particle's starting position, and have introduced

$$[\widetilde{\Delta t}](z|z_0) = \int_{z_0}^{z}\frac{dz'}{v(z')} \quad \text{and} \tag{8}$$

$$\left[\frac{\widetilde{\Delta t}}{\tau}\right](z|z_0) = \int_{z_0}^{z}\frac{dz'}{\tau(z')v(z')}. \tag{9}$$

D. Transport equation for the first-generation density

If, instead of exciting a single electron, a distributed source of excited electrons is present, the total first-generation flux at time t through a surface in z due to all electrons with spin σ and energy E is

$$\Phi^{[1]}(z,t) = \int_{-\infty}^{+\infty}dz_0\int_{-\infty}^{t}dt_0\,S^{\text{ext}}(z_0,t_0)\phi_\delta(z,t|z_0,t_0), \tag{10}$$

where $S^{\text{ext}} = S^{\text{ext}}(\sigma,E,z,t)$ is the electron source term that has to be computed from the spatial and temporal profile of the laser and the absorption probability. We define the operator $\hat{\phi}$, $\hat{\phi}S^{\text{ext}} \equiv \Phi^{[1]}$.

Having computed the flux, it is possible to write down a continuity equation for the density of first-generation electrons. A general (1D) continuity equation is

$$\frac{\partial n^{[1]}}{\partial t} = -\frac{\partial\Phi^{[1]}}{\partial z} - R(n) + S^{\text{ext}}, \tag{11}$$

where Φ is the flux, R is a reaction term, and S a source term. In this case, the reaction term is simply $R(n) = n^{[1]}(\sigma,E,z)/\tau(\sigma,E,z)$, i.e., the number of first-generation electrons that become second generation after being scattered, for every spin and energy and at every position. Hence the complete transport equation specific to this case is

$$\frac{\partial n^{[1]}}{\partial t} = -\frac{\partial\hat{\phi}S^{\text{ext}}}{\partial z} - \frac{n^{[1]}}{\tau} + S^{\text{ext}}. \tag{12}$$

Note that in standard diffusion the flux term is linked to the density, whereas in this case the flux is linked to the source term only.

E. Transport equation for the total density

Next, we want to describe what happens after the first scattering event. Using the assumption that incoming and outgoing directions are uncorrelated, we can notice that the particle after being scattered behaves actually as if being excited by an effective source,

$$S^{[2]} = \sum_{\sigma'}\int p(\sigma,\sigma',E,E',z)\frac{n^{[1]}(\sigma',E',z,t)}{\tau(\sigma',E',z)}dE', \tag{13}$$

which is the scattering term at all energies weighted by the transition probability after a scattering, $p(\sigma,\sigma',E,E',z)$. This quantity treats inelastic and elastic scattering events and electron cascades, as discussed further below. We define the operator $\hat{\mathcal{S}}$ as $\hat{\mathcal{S}}n^{[1]} \equiv S^{[2]}$. Note that if $\int p(E',E,z)dE' < 1$, we are implicitly assuming that a part of the scattered electrons are stopped, in other words, scattered to states with negligible mobility. The second-generation electron density will then

obey

$$\frac{\partial n^{[2]}}{\partial t} = -\frac{\partial \hat{\phi} S^{[2]}}{\partial z} - \frac{n^{[2]}}{\tau} + S^{[2]}. \tag{14}$$

Applying the same procedure we obtain the equation for the density of the third-generation electrons $n^{[3]}$, and so on. Summing up everything we derive the transport equation for the full (spin) density $n(\sigma,E,z,t)$:

$$\frac{\partial n}{\partial t} + \frac{n}{\tau} = \left(-\frac{\partial}{\partial z}\hat{\phi} + \hat{I}\right)(\hat{\mathcal{S}} n + S^{\text{ext}}), \tag{15}$$

where $\hat{I}$ is the identity operator and $n = \sum_{N=1,\infty} n^{[N]}$. Since Eq. (15) has to be satisfied for every value of σ and E, we effectively have a set of coupled equations.

Equation (15) is a first central result, the transport equation governing the dynamics of laser-excited NEQ electrons. Its numerical solution will be described further below. Note that the transport equation defines the time-dependent motion of the NEQ electron density as well as the magnetization dynamics of the laser-excited electrons, through the difference of the spin components $[M(E,z,t) = 2\mu_B(n(\uparrow,E,z,t) - n(\downarrow,E,z,t))]$.

F. Analysis of regime of laser-induced transport

An important aspect of all forms of transport is to which transport class they belong. Our aim is to compare here the regime of NEQ laser-induced electron transport to the well-known ballistic and diffusive transport regimes. This is, however, a more involved task, as the above-developed transport model treats the complex interplay of several physical effects that are occurring during and after the excitation by a femtosecond laser pulse, and until a defined electronic temperature is established in the system, on an equal footing. Specifically, on this timescale the transport and thermalization of laser-excited electrons cannot be decoupled and have therefore been included within the same formalism. The two standard limits of transport, ballistic and diffusive thermal transport, are essentially different in the crucial aspect that these *do not include electron-thermalization effects*.

Nonetheless, to compare the NEQ laser-induced transport to these two standard limits, we artificially decouple the electron thermalization. To this end, we study here an artificial system of particles where only transport takes place and no thermalization. The quantity governing both the elastic and inelastic electron scattering probabilities is $p(\sigma,\sigma',E,E',z)$ introduced in Eq. (13). We assume all particles to have a fixed group velocity and (elastic) lifetime and that all electron scatterings are purely elastic. This condition is equivalent to assuming p to be diagonal in energy, i.e., upon a scattering event the particle is emitted with probability 1 to the same energy. We also assume that the particles diffuse in an infinite homogeneous material.

Next, we may right away note that already under this decoupling the regime of laser-induced NEQ particle transport is different from the two standard limits of transport, ballistic and diffusive thermal transport. In the latter regime, a traveling particle undergoes infinitely many scatterings within a time interval whereas in the former regime it undergoes zero scatterings. Laser-generated NEQ electrons, however, undergo a limited, nonzero number of scatterings. Within the field of anomalous diffusion, the different regimes are characterized by the variance σ^2 of the displacement of a single-particle distribution (or equivalently the particle distribution for a Dirac δ source in space and time) as a function of time,

$$\sigma^2(t) = \int n(t,z)(z - z_0)^2 dz, \tag{16}$$

also called dispersion. Note that Eq. (16) computes only the dispersion on the z axis, while the motion the particle undergoes is instead fully three dimensional.

Standard thermal diffusion processes that are governed by Brownian motion are characterized by a σ^2 that grows linearly with time:

$$\sigma^2(t) = K_w t^{2/d_w}, \tag{17}$$

with $d_w = 2$, where K_w represents the generalized diffusion coefficient and d_w is called the anomalous diffusion exponent.[62,63] In ballistic diffusion, the particle distribution spreads with the constant velocity and is characterized by $d_w = 1$. Solving the governing transport equation (15) for the artificial above-introduced model system shows that the developing electron motion falls in the category of superdiffusive processes $1 \leqslant d_w < 2$. But as a major improvement over the commonly used superdiffusion models,[63] where the anomalous diffusion exponent d_w is assumed constant in time, the transport defined by our Eq. (15) has an appropriate time-dependent d_w to capture the motion of a particle scattering a finite number of times. In Fig. 2, we plot the computed time evolution of $d_w(t)$ defined as

$$d_w(t) = \frac{2}{t}\frac{\sigma^2}{d\sigma^2/dt}, \tag{18}$$

for the introduced model system. The curves show the time evolution of the anomalous diffusion coefficient for a particle moving with constant velocity and undergoing only elastic scatterings with lifetime $\tau = 10$ or 40 fs. Note that $\tau = 40$ fs is a reasonable estimate of the elastic electron scattering lifetime in d metals.[64,65] One can observe that for short times, $t \ll \tau$, the motion is essentially ballistic $[d_w(t) \approx 1]$, because

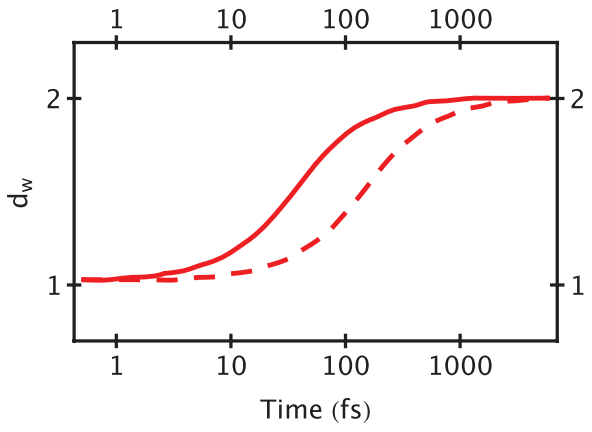

FIG. 2. (Color online) Time evolution of the anomalous diffusion coefficient d_w as defined in Eq. (17), numerically computed for a particle with constant velocity and an elastic lifetime $\tau = 10$ fs (full curve) or $\tau = 40$ fs (dashed curve).

on this timescale the particle experiences approximately no scatterings. If instead one focusses on times $t \gg \tau$, the lifetime becomes essentially negligible compared to the analyzed timescale and the overall motion is well approximated by standard diffusion [$d_w(t) \approx 2$]. The crossover from nearly ballistic to diffusive happens through the increasing number of scatterings that randomize the velocity direction. Note also how models in the superdiffusive regime with constant, time-independent d_w fail at all times in describing the laser-induced NEQ particle transport.

For the general case, the electron-thermalization effect has to be included as well and the simple time evolution of the anomalous diffusion coefficient for a nonthermalized particle in Fig. 2 will accordingly become modified. It will, in addition, become both material and geometry dependent. In typical d metals, the electron-thermalization process is known to take place within some 500 fs.[46–49] Through the equilibration energetic electrons in these metals loose energy and are sent into less mobile d bands, which substantially reduces their contribution to the transport. In order not to neglect the thermalization effect, it is evident that the femtosecond laser-induced spin transport taking place in the superdiffusive regime needs to be described by our Eq. (15). We further note that the time frame of the superdiffusive transport is also precisely the time frame in which the ultrafast laser-induced demagnetization is accomplished in 3d metallic ferromagnets.[17,66–68]

G. Totally reflecting surface

As a subsequent step, we want to include the presence of surfaces in the model. If we assume that on reflection at a surface with the vacuum the electron is bounced back completely elastically, then its motion is just the motion it would have had if it were not reflected but mirrored with respect to the surface. This situation is schematically depicted in Fig. 3. It is then straightforward to describe a totally reflecting surface, simply by mirroring the whole system (source included), solving the transport equation for the extended system and afterwards considering only the physical part (see Fig. 3).

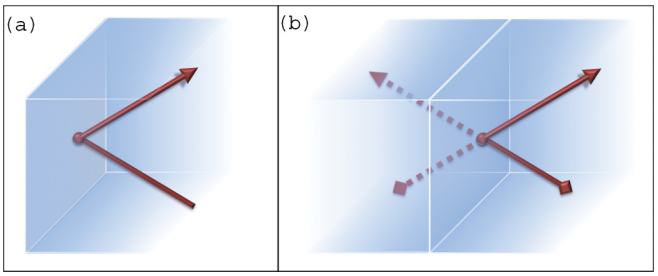

FIG. 3. (Color online) A totally reflecting surface causes an electron to elastically bounced back (a). This situation is equivalent to the case (b) where another electron is created in a mirrored auxiliary system and emitted in a mirrored direction. Since we assumed the source to emit isotropically, the mirrored source behaves as the real one but it is located at the mirrored position.

H. Particle accumulation

To keep track of the displacement of the electrons, we have to compute the number of electrons that are excited and eventually sent back to nonmobile states at later times and positions. Addressing each generation at a time we can say that the source term removes electrons from bands below the Fermi energy, while the scattering term inhibits electrons. The change in the population of bands below the Fermi energy $n^{[i]}_{<E_F}$ induced by the ith generation is

$$\frac{\partial n^{[i]}_{<E_F}}{\partial t} = \int \left(-S^{[i]} + \frac{n^{[i]}}{\tau} \right) dE. \tag{19}$$

Summing up contributions from all generations gives the total change:

$$\frac{\partial n_{<E_F}}{\partial t} = -\int S^{\text{ext}}(E')dE' + \int \left[1 - \int p(E',E)dE \right] \frac{n(E')}{\tau(E')} dE'. \tag{20}$$

It is then straightforward to compute for every position the total electron (or spin) density variation as the sum of electrons excited above and the change of the population below the Fermi energy:

$$\Delta n_{\text{tot}} = n + \Delta n_{<E_F} = n + \int \frac{\partial n_{<E_F}}{\partial t} dt. \tag{21}$$

IV. ANALYTICAL SOLUTION FOR THE FIRST GENERATION

It is possible to compute the electron density for the first generation analytically in some cases. We consider here such case to elucidate the occurring processes. For simplicity, we will assume that the electrons after the first scattering are completely stopped and therefore sent to a band below the Fermi energy.

A. Homogeneous material

The case of an infinite homogeneous material is the simplest one. Equations (8) and (9) become simply

$$[\widetilde{\Delta t}](z|z_0) = \frac{z - z_0}{v}, \quad \left[\frac{\widetilde{\Delta t}}{\tau} \right](z|z_0) = \frac{z - z_0}{\tau v}. \tag{22}$$

The flux kernel in Eq. (7) is now simple and $\hat{\phi} S$ can be written as a convolution:

$$\hat{\phi} S = (\phi * S)(z,t) = \int dz_0 \int dt_0 \, \phi(z - z_0, t - t_0) S(z_0, t_0). \tag{23}$$

Integrating Eq. (12) for a point source pulse [$S^{\text{ext}}(z,t) = \delta(z - z_S, t - t_S)$], we obtain the Green's function

$$n^{[1]}_{\delta}(z - z_S, t - t_S) = \frac{1}{2v} \frac{1}{t - t_S} \exp\left(-\frac{t - t_S}{\tau} \right) \Theta\left(t - t_S - \left| \frac{z - z_S}{v} \right| \right) \tag{24}$$

that represents the electronic density given by the point source pulse. We can write the electron density up to the first scattering for a general source as

$$n^{[1]}(z,t) = \left(n_\delta^{[1]} * S\right)(z,t). \tag{25}$$

We are, however, interested in the total electron density $n^{[1]}_{\mathrm{tot},\delta} = n^{[1]}_\delta + \Delta n^{[1]}_{<E_F,\delta}$, Where

$$\Delta n^{[1]}_{<E_F,\delta} = -\delta(z - z_S) + \frac{1}{2v\tau}\left[E_1\left(\frac{t - t_S}{\tau}\right) - E_1\left(\left|\frac{z - Z_S}{v\tau}\right|\right)\right] \Theta\left(t - t_S - \left|\frac{z - z_S}{v}\right|\right), \tag{26}$$

with $E_1(x)$ being the exponential integral function. Figure 4(a) shows the behavior of the introduced functions. Panel (a.1) gives the time evolution of the excited electron density. Immediately after the excitation, it has a δ-like shape because all excited electrons are located at the same point. As time evolves, two effects are evident: the density spreads in space and decreases in magnitude. At this point, it is instructive to note the wavefront traveling: in a standard diffusion model the tail would have extended to infinity immediately. The electron density is indeed in the here-discussed analytical solution exactly a step function. This originates from the fact that, after the excitation by a point source pulse, electrons will start spreading by staying uniformly on the surface of a sphere with a radius growing in time. If we project the surface of the sphere on an axis at a given time we can observe a steplike behavior. Finally, the electron density decreases in time—this is both due to the spreading and to the scattering events. Computing the area below the curve gives an exponential decay of the area, i.e., $\int_{-\infty}^{+\infty} n^{[1]}_\delta(z,t)dz = e^{-t/\tau}$.

Figure 4(a.2) depicts the electron density below the Fermi energy. At $z = 0^+$, there is the $-\delta$-like depletion left by the source pulse that removed electrons from states below the Fermi energy. As time proceeds, excited electrons are scattered and transferred back to levels below the Fermi energy (since computing the diffusion for the first generation only is equivalent to assuming that after a scattering electrons are completely stopped), giving a positive contribution to this density. Computing the area below this function gives $\int_{-\infty}^{+\infty} n^{[1]}_{<E_F,\delta}(z,t)dz = -e^{-t/\tau}$. This means that for $t \to \infty$ all electrons are again deposited back in the states below the Fermi energy even if being positioned at different z's. The last panel (a.3) of the first row in Fig. 4 shows simply the total electron density. The area is exactly zero since effectually no electrons are destroyed nor created but are simply displaced. One may note that the material, even if globally neutral, seems to be locally charged; we will discuss this effect in Sec. V A.

B. Totally reflecting surfaces and heterostructures

As mentioned before, the presence of a totally reflecting surface at $z = z_{\mathrm{sf}}$ can be included in the Green's function of the problem through

$$n^{[1]}_{\delta\,\mathrm{sf}}(z - z_S, t - t_S) = n^{[1]}_\delta(z - z_S, t - t_S) + n^{[1]}_\delta(z - 2z_{\mathrm{sf}} + z_S, t - t_S). \tag{27}$$

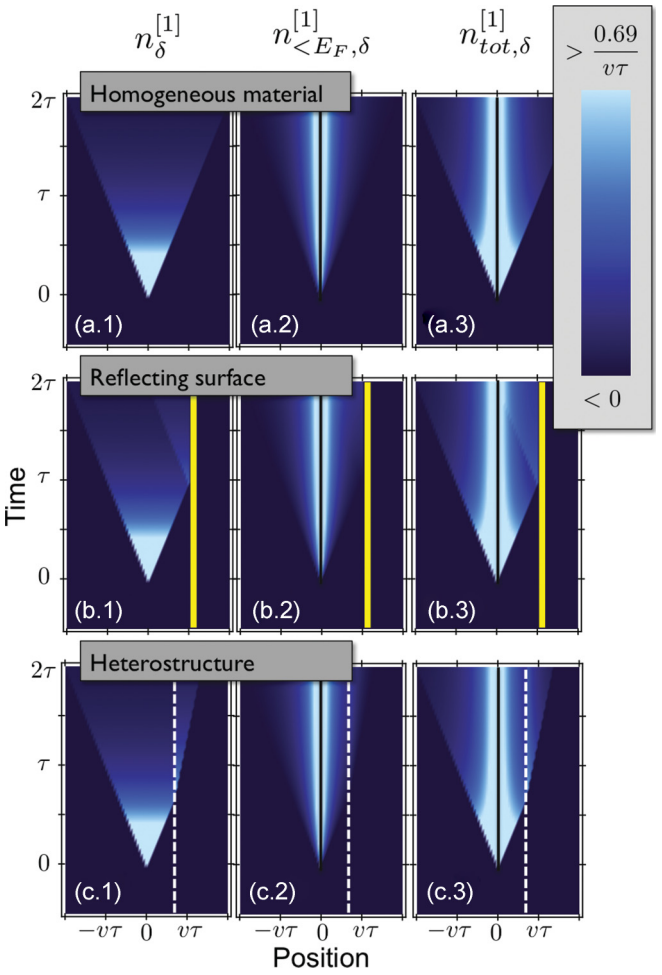

FIG. 4. (Color online) Analytically computed position-time intensity profile of the density of excited *first-generation only* electrons $n^{[1]}_\delta$ (left-hand panels), the change of density of electrons below the Fermi energy $n_{<E_F,\delta}$ (central panels) and the their sum (right-hand panels) for the case of a Dirac δ source in time and space. Bright areas indicate high intensities, dark areas low intensities. The depth z dependence is on the abscissae, expressed in units of $v\,\tau$, while the time t dependence is on the ordinates in units of τ. The top row (a) refers to the case of a homogeneous material. The middle row (b) displays the case of a homogeneous material with a perfectly reflecting surface (the position of which is highlighted by a yellow thick line) at $z_S = v\,\tau$. The bottom row (c) shows the case of a heterojunction made of two different metallic materials. The area for $z > 0.7\,v\,\tau$ represents the second material with $v_2 = 0.5\,v$ and $\tau_2 = 0.5\,\tau$. The interface between the two materials is highlighted by a thin broken white line.

Figure 4(b) depicts the effect of a totally reflecting surface in a homogeneous material. At negative times, all excited densities are zero. For positive times and as long as the electrons don't reach the surface, the behavior is the same as that in a homogeneous material. However, after reaching the surface, electrons are reflected and the reflected electron density adds up to the one evolving as in a homogeneous material.

The case of heterogeneous systems is more complicated but an explicit expression for the first-generation density given by a point source pulse can be given. As this is

a rather lengthy expression, we omit it here. Instead, we visualize in Fig. 4(c) the influence of the presence of two different metallic materials. As in the previous case for times before the electrons reach the second metallic layer no anomalous behavior appears. But when the wavefront crosses the heterojunction's interface, its propagation velocity changes and the constant-in-space shape is destroyed. This is due to the fact that, after crossing the interface, electrons are not traveling anymore on a sphere (not even one with a different radius), but on a complex three-dimensional surface.

V. APPROXIMATIONS

In the following, we summarize all approximations that have been made in the derivation. First, we analyze the influence of screening of the NEQ electron flow, and subsequently, in Secs. V B–V D, we discuss the approximations that are not directly related to the derivation of the model, but have to be made only when suitable *ab initio* data are missing.

A. Screening of the charge current

As already pointed out, an electric field has to be extremely high to be effective on the superdiffusive motion of electrons. Standard electric fields are far too weak to cause, through the bending of the electron trajectory with respect to the straight trajectory in the absence of the field, a displacement that would be appreciable compared to the total displacement. However, under certain experimental conditions (for instance, the case of ultrafast demagnetization experiments with an almost complete demagnetization) the electric field that would have been induced by the local charges created by the separation of electrons and holes is indeed big. In this situation another kind of motion comes into play.

Dielectric screening in metals is a well-known effect.[69] In metals the screening is complete, and electrons will immediately flow to surround (escape) the positive (negative) charge. The bare Coulomb potential of an extra fixed point charge is then modified into a screened Coulomb potential that is cut off at a characteristic distance of the order of k_F^{-1}. After the screening is completed, the electric potential will be negligible at distances of few lattice lengths. Also, the screening proceeds almost instantaneously compared to the considered femtosecond timescale. A recent experiment[61] showed that screening times for transition metals are indeed very short (<2 fs).

At this point, it is useful to analyze which electrons are contributing to the screening effect: electrons from around the Fermi energy are involved (as well as holes created in the valence band). Unless the laser-excitation is very large, the electrons that are involved in the superdiffusive motion form just a small fraction and the greatest part of the screening is done by other electrons. It is then a good approximation to assume that the screening is done entirely by electrons from around the Fermi energy and that the contribution from superdiffusing electrons is negligible. Equivalently, this means that the effective electric field felt by superdiffusing electrons is negligible.

Notably, in magnetic metals the situation is different, as for these, the screening effect can cause spin transport, because the screening electrons are spin polarized. A question is then what is the contribution to the screening that originates from the individual spin channels. Taking Ni as an example, it is known that the screening in Ni is accomplished mainly by spin-minority carriers, in fact, it has been experimentally shown that a considerable screening demagnetizes the atom almost completely.[70] This is easily understood considering that the partial density of states (DOS) at the Fermi energy for spin-minority electrons is much larger than that of the spin-majority ones.

One can roughly estimate that the spin polarization of the dielectric screening in the case of a Ni film on Al, treated in Ref. 29 will enhance the demagnetization. Even so, the contribution to the magnetization dynamics is expected to be small since the transfer will displace magnetization only from neighboring atoms. It is then easy to imagine that in the case of a homogeneous excitation, the magnetization displacement induced by this effect will vanish exactly, hence it becomes of importance only where there are highly unhomogeneous excitations or interfaces between materials. In view of the marginality of this effect and the lack of quantitative estimations, we prefer to ignore the screening-induced magnetization flux and assume simply a non-spin-polarized screening flow. Within this approximation, the only effect of the dielectric screening is to cancel the charge transfer, but no contribution to the spin transport will occur.

B. Description of the motion

One of the required quantities is the probability to have an electron-phonon or electron-impurity scattering event. Electron-phonon scattering cross sections can be evaluated *ab initio*,[31,35] but unfortunately the one for electron-impurity scatterings depends strongly on the experimental preparation of the sample. Well-annealed materials will have a low defect concentration and low electron-impurity scattering cross section, whereas nanostructured films will, for example, have a large cross section for that type of scatterings. Even experimentally it is not easy to characterize a sample from this point of view.[71] Fortunately, as already pointed out in Ref. 29, even large variations in inelastic scattering probabilities do not affect notably the result and a precise knowledge is needed only if very precise results are required.

Conversely, for the case of electron-electron scatterings, the resulting spin- and electron-dependent lifetimes can be computed *ab initio*.[65,72,73] The used *ab initio* data from *GW* calculations[65,72] do not provide values for the low-energy range and an extrapolation had to be done. Even though the Fermi liquid divergence of lifetimes at the Fermi energy does not happen in real materials and hence the lifetimes should converge to a finite value at the Fermi energy, we don't have a good estimation for this value. Henceforth, the extrapolation for the lifetimes has been done in a conservative way with the main aim of being on the safe side (thus underestimating the superdiffusion) instead of with the aim of being precise. In Fig. 5, we show the values used for Ni and Fe where the lifetimes at low energies have been obtained by simply

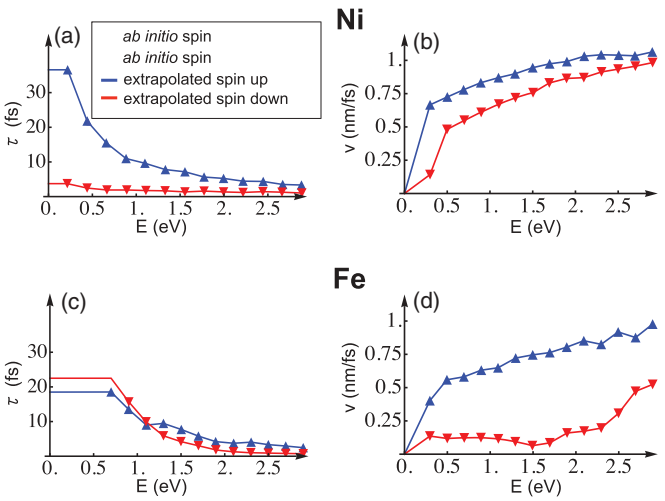

FIG. 5. (Color online) The *ab initio* calculated electron lifetimes and velocities in Ni and Fe, taken from Ref. 65. Blue triangles up refer to spin-majority and red down triangles to spin-minority carriers. The blue and red lines show the extrapolation of the data as used in the present work for spin-majority and minority carriers, respectively. The top panels depict the lifetimes (a) and velocities (b) for Ni, the bottom panels (c) and (d) for Fe.

assuming a constant energy dependence. A discussion of the effect of different extrapolations can be found in Ref. 29.

The velocities have been extrapolated to zero at the Fermi energy. This is due to the fact that close to the Fermi energy, electron and holes in the same spin channel have approximately the same transport properties, while transporting opposite spin. This means that the closer the electron-hole pair is to the Fermi energy the more they diffuse in the same way and cancel reciprocally the net spin transport. Since we have neglected the hole transport, we cannot obtain this cancelation around the Fermi energy and we have to enforce it by assuming zero velocity at the Fermi energy (see Fig. 5).

During the superdiffusive transport, the electron thermalization process (and hence the change in energy of the traveling electrons) is to be taken into account. This is done here as follows: in the situation that the hot NEQ electron scatters with a phonon or an impurity, it is a good approximation to suppose the scattering to occur completely elastically since the electron energy loss per such scattering is much lower than the one in electron-electron scattering, leading to the probability function $p_{\mathrm{el}}(\sigma,\sigma',E,E') = \delta_{\sigma\sigma'}\,\delta(E-E')$ (the dependence on z is suppressed for sake of brevity).

For the electron-electron scatterings, however, the probability distribution of the final energy of both the scattered and the recoil electron is needed and these cannot be approximated as elastic. A fully *ab initio* calculation of the final energy probability distribution is, to our knowledge, currently not available. Hence we have approximated such scattering event using the classical description of a two-particle scattering process. When two particles with masses m_a and m_b, and velocities v_a and $v_b = 0$, respectively, scatter the maximum energy transferred can be written as

$$\Delta E_{\max} = \frac{4m_a m_b}{(m_a+m_b)^2}E', \tag{28}$$

where E' is the energy of the incoming electron. To avoid the introduction of parameters, we assumed a uniform probability density in energy, ranging from $E'-\Delta E_{\max}$ to E' for the final energy of the incoming electron. Consistently, we assumed that the energy lost by the incoming electron is, in this equilibration process, transferred to the other electron at the Fermi energy that will now be excited and begin to contribute to the transport. An important value is also the probability to oust an electron with a particular spin. To avoid free parameters, we assumed that both spin-up and spin-down electrons have the same probability to be excited from the Fermi energy after an electron-electron scattering. The expression for the probability in this case is

$$p_{\mathrm{in}}(\sigma,\sigma',E,E') = \delta_{\sigma\sigma'}\frac{\Theta_{[E'-\Delta E_{\max},E']}(E)}{\Delta E_{\max}} + \frac{1}{2}\frac{\Theta_{[0,\Delta E_{\max}]}(E)}{\Delta E_{\max}}, \tag{29}$$

where the function Θ is the unit step, which is 1 when the argument is inside the interval specified in the square brackets. Note that zero energy corresponds to the Fermi energy of the unperturbed system.

Combining the two different types of scatterings the total probability expression is computed as

$$p = \frac{\tau_{\mathrm{el}}}{\tau_{\mathrm{el}}+\tau_{\mathrm{in}}}\,p_{\mathrm{in}} + \frac{\tau_{\mathrm{in}}}{\tau_{\mathrm{el}}+\tau_{\mathrm{in}}}\,p_{\mathrm{el}} \tag{30}$$

with all the τ's evaluated at (σ',E').

C. Neglecting of Auger electrons

A further contribution to the number of electrons participating in the superdiffusion may come from the generation of Auger electrons (in our case electrons that are excited above the Fermi energy and not above the work function of the metal by the de-excitation of a hole). This will act as a delayed source of excited electrons. It can easily be included in the model, but at this stage we neglected entirely this effect.

D. Time-independent materials properties

An approximation that we expect to become increasingly poor with the increase of the laser fluence is the assumption that all the properties of the materials are constant. For example, the pronounced spin dependence of the excited electron lifetimes and velocities is due to the ferromagnetic polarization in the material. However, during the demagnetization process the spin polarization of the electronic population in the material is changed. For small demagnetizations this will affect negligibly the values of the spin-dependent lifetimes, but this can no longer be expected for sizable demagnetizations. The way in which the lifetime and velocity values are going to be altered by the new spin population is not easy to predict. The functions in Eqs. (8) and (9) will, as a result, acquire a functional dependence on $n(z,t)$ as well as the operator $\hat{S}$ and the flux kernel $\hat{\phi}$. Consequently, the transport equation, Eq. (15), governing the superdiffusive flow will clearly not be a linear equation any more.

So far we have neglected this nonlinear effect, but we stress that it nonetheless intuitively explains an important

experimental observation: a total demagnetization was never seen (the maximum demagnetization observed[74,75] so far saturated around 90%). The closer the system is to the completely demagnetized state the lesser effective is the superdiffusive spin transport in demagnetizing it further and a complete demagnetization can therefore not be obtained.

VI. NUMERICAL IMPLEMENTATION

The numerical implementation of the derived transport equations has been mostly done using standard techniques[76] apart from a few details that will be pointed out in the following.

A. Discretization grids

The easiest way to discretize the time in the superdiffusive transport equation (15) is to use an Euler forward method,

$$n(E,z,t+\Delta t) = \left(1-\frac{\Delta t}{\tau}\right) n(E,z,t) + -\Delta t \left(\frac{\partial}{\partial z}\hat{\phi} + \hat{I}\right) \times [\hat{\mathcal{S}} n(E,z,t) + S^{\text{ext}}(E,z,t)], \quad (31)$$

with Δt the discretization step on the temporal axis. As is well known, this method has a first-order convergence in time. For a second-order convergence in time, one has to use the implicit Crank-Nicolson algorithm. Unfortunately, the implicit equation is very difficult to solve and one moreover has to solve it remembering that Eq. (15) stems from the summation of single-generation equations [see Eq. (14)]. These contributions decay fortunately as $(1-p)^N$ and therefore one can compute just a finite number of generations.

The discretization in space is done on a uniform grid with step Δz. For achieving a second-order convergence in space and a better stability of the numerical solution, the derivative of the flux in Eq. (31) is computed by finite difference approximation on a second grid shifted by $\Delta z/2$ with respect to the main one:

$$\frac{\partial \hat{\phi}\hat{\mathcal{S}} n(E,z,t)}{\partial z} = \frac{\hat{\phi}\hat{\mathcal{S}} n\left(E,z+\frac{\Delta z}{2},t\right) - \hat{\phi}\hat{\mathcal{S}} n\left(E,z-\frac{\Delta z}{2},t\right)}{\Delta z}. \quad (32)$$

Note that in order to compute the right-hand term of Eq. (32), the functions in Eqs. (8) and (9), used in the definition of the flux, have to be computed with the second argument on the main spatial grid but with the first one on the shifted grid.

Finally, the discretization of the energy E is done on an uniform grid with step ΔE, using typically 12 energy channels in the excited energy interval of 0 to the pump laser energy (here assumed to be 1.5 eV). The energy integration is done by a simple rectangle method.

B. Flux operator

For the discretization of the flux term in Eq. (10), one has to face the divergence that the flux kernel in Eq. (7) exhibits at $t \to t_0$. It is, however, easy to show that

$$\hat{\varphi} S(E,z,t) = \int_{-\infty}^{+\infty} dz_0 \int_{-\infty}^{t'} dt_0\, S^{\text{ext}}(z_0,t_0)\phi(z,t|z_0,t_0) + \mathcal{O}[(t-t')^2]. \quad (33)$$

This implies that the numerical time integration of Eq. (10) can be carried out up to the time $t-\Delta t$, avoiding the divergence and achieving a first-order convergence.

VII. WORKED EXAMPLES FOR LAYERED HETEROSTRUCTURES

In the following, we report numerical simulations for the laser-induced NEQ transport and spin dynamics in typical heterostructures, a ferromagnetic/nonmagnetic metal junction (specifically, Ni/Al and Fe/Al) and a ferromagnetic metal/nonmagnetic insulator junction (e.g., Ni/MgO and Fe/MgO).

For the insulator, the band gap is assumed sufficiently large that no excited electrons can penetrate the insulator. Accordingly, the interface ferromagnet/insulator has hence been treated as a perfectly reflecting surface. In the performed simulations, the hybrid junctions are excited from the ferromagnet's side by a 40-fs laser pulse. As an outcome of the simulations we predict distinct differences in the behaviors of both the ferromagnets Ni and Fe in the two cases of metallic or insulating junctions.

We stress therefore that superdiffusive spin transport is very sensitive to changes of the geometry and material. For instance, adding capping layers or changing the thicknesses of the layers in the simulations below can change amply the predicted demagnetization.

A. Ni/Al and Ni/MgO hybrid junctions

Figure 6 shows the superdiffusive spin-polarized electron flow and effective demagnetization on the femtosecond time scale for the Ni-based junctions. The Ni layer is assumed to be 10 nm thick and it is excited by a laser at 1.5 eV depositing an average of 0.1 photons per Ni atom. The ratio of excited majority- to minority-spin electrons, have been taken from *ab initio* calculations.[58] Coming to the results, we can recognize from Figs. 6(a) and 6(d) that, for both metallic and insulating substrate layers, after the laser excitation both majority and minority carriers are excited to Ni's conduction bands. However, on account of the spin-dependent lifetimes minority-spin electrons are slowed down rapidly and within 100 fs decay to (almost) nonmobile bands approximately at the position where they were excited. Instead, majority-spin electrons have longer lifetimes and higher velocities. In the case of the Al substrate [see Fig. 6(a1)] they diffuse away fast from the excitation region after being created, driving part of the demagnetization process [see Fig. 6(b)]. A second part of the demagnetization is driven by the back flux of spin-minority electrons from the Al substrate. The laser excitation tail and the electrons escaped from the Ni layer experiencing inelastic scatterings in the Al substrate and excite electrons

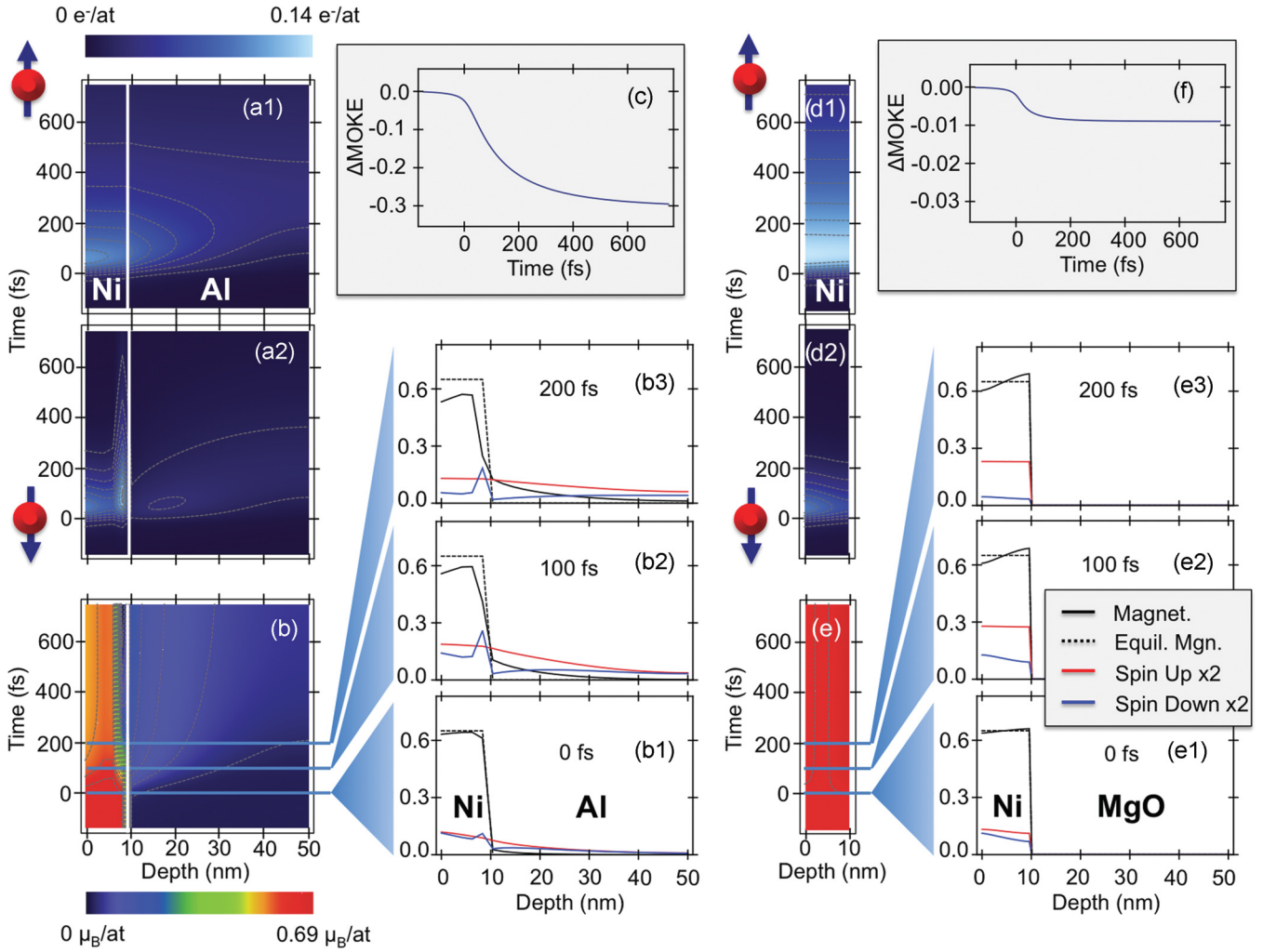

FIG. 6. (Color online) Comparison of ultrafast laser-induced spin-dynamics in Ni on different substrates. Panels on the left-hand side show the case of 10 nm of Ni grown on Al, computed for excitation by a laser of 1.5 eV photon energy and an average number of photons absorbed per Ni atom of 0.1. Panels on the right-hand side display the case of a 10-nm Ni film grown on an insulating substrate like MgO. For each case, following the panels in a counterclockwise order and starting from the one at the top left corner, we show the majority-spin electron density, the minority-spin electron density, the magnetization density, three snapshots at three different times and, finally, the normalized MOKE signal change (top-right panel).

that have again a random velocity direction. A fraction of these electrons establish a flux from Al to Ni. Spin-majority electrons entering the Ni layer continue diffusing, but spin-minority electrons experience a considerable worsening of the transport properties as soon as they enter the ferromagnetic layer. The consequence is that they are trapped right after the interface [see, for instance, the reduction of the magnetization and the peak in the minority-spin density at a depth between 8 and 10 nm in Fig. 6(b3)].

Conversely, in the case of the insulating substrate [see Fig. 6(d1)] spin-majority electrons are redistributed almost uniformly within the Ni layer. This is intuitively understandable since the total distance traversed by these electrons, before the thermalization is completed, is much longer than the layer thickness. That, along with the randomness introduced by the time position of the scattering and the emission direction after it, explains the almost uniform spreading. Henceforth the resulting femtosecond demagnetization profile [see Fig. 6(e)] in this case follows approximately the shape of the majority-spin depletion distribution, i.e., the spatial intensity distribution of the laser. One can observe that the average magnetization of the Ni layer as a whole is unchanged, since we do not assume any spin-dissipation channel and no spin-polarized electron could escape. Yet, the region close to the surface to the vacuum has been demagnetized, already after 100 fs, which is compensated by the increase of magnetization at the metal/insulator interface [see Fig. 6(e3)]. A remark appropriate at this point is that lateral superdiffusive outflow of NEQ electrons will occur as well, but has not been included in the present modeling.

If now both hybrid junctions are probed using a magneto-optical probe (e.g., magneto-optical Kerr effect, MOKE) in reflection, the magneto-optical sensitivity decays rather quickly away from the vacuum surface. Supposing that the

probe laser has a penetration depth λ then the measured Kerr rotation change with respect to the unperturbed rotation will be

$$\frac{\Delta\theta_L - \Delta\theta_u}{\Delta\theta_L} = \frac{\int m(z) e^{-\frac{z}{2\lambda}}\, dz - m_u \int e^{-\frac{z}{2\lambda}}\, dz}{m_u \int e^{-\frac{z}{2\lambda}}\, dz}, \quad (34)$$

where $\Delta\theta_u$ is the Kerr rotation measured in the unperturbed case, $\Delta\theta_L$ the one after the laser excitation, $m(z)$ is the position-dependent magnetization profile after the laser excitation and m_u is the unperturbed (uniform) magnetization of the material. Note that we assume here that the MOKE signal of the laser-excited material follows the atomic magnetization linearly as for the unperturbed material, which might not always be the case.[58,77]

Figures 6(c) and 6(f) exhibit the predicted time dependence of the normalized femtosecond MOKE signal change for the Al and insulating substrates. In the latter case, the maximum change in the MOKE signal is severely reduced compared to the former case, but it is still present. An interesting feature which can be extracted from these simulations is that the demagnetization times of the metallic and insulating heterostructures are different: by fitting the demagnetization curves with a simple exponential decay, i.e., $[M(t) - M(0)]/M(0) \approx -(1 - \Delta M_{\mathrm{MAX}} e^{-t/\tau_M})$, one can extract approximate demagnetization times τ_M. For the Ni/Al bilayer structure ($\tau_M \approx 160$ fs), spin-polarized cascade electrons cause an enhanced demagnetization by diffusing quickly away from the Ni film, whereas for Ni on the insulating MgO substrate the spatial inhomogeneity of the excitation, which drives the demagnetization, fades away quickly ($\tau_M \approx 60$ fs) after the first generation. Hence the resulting demagnetization is smaller and it is effective approximately only as long as the pump laser-pulse is active plus the majority-spin electron's lifetime.

In the x-ray regime, the penetration depth is different. Considering the x-ray magnetic circular dichroism (XMCD) at the Ni L edges, one would expect to measure an even smaller transient demagnetization signal for the case of a Ni layer on the insulator. As x rays still have a finite penetration depth the demagnetization will be much smaller than in the case of the metallic Al substrate.

The mechanism of ultrafast demagnetization occurring in the Ni layer on metallic substrate has been outlined previously[29]—spin-angular momentum is removed from the Ni layer through superdiffusive motion of the excited hot electrons. This spin transfer process proceeds on the timescale of the superdiffusive flow, causing a typical demagnetization time of some 300 fs. Concomitant with the Ni layer's demagnetization is the spin current entering the Al substrate [see Figs. 6(b2) and 6(b3)]. A smaller percentage of the less mobile spin-minority electrons also penetrates the Al layer. Note that both the spin-majority and minority currents are fully screened and are therefore pure spin currents. However, the *net* spin-transfer current is about 90% at 200 fs for the Ni/Al heterostructure. Note that a higher net spin polarization can be obtained by using a thicker Ni layer.[29]

B. Fe/Al and Fe/MgO hybrid junctions

The transient spin-polarized electron dynamics has been computed, too, for Fe/Al and Fe/MgO heterostructures. It is instructive to compare the spin dynamics and demagnetization to those obtained for the Ni-based systems. The computed demagnetization times of Fe/Al and Fe/MgO are $\tau_M \approx 130$ and 45 fs, respectively, obtained again by fitting the calculated curves with simple exponential decays (in the case of the Fe/MgO heterostructure an exponential recovery has been included in the fitting as well). Importantly, the spin-lifetimes of excited electrons are different from those in Ni,[65] and the asymmetry between the two spin components is smaller in Fe. From the results shown in Fig. 7 it can be observed that the process of demagnetization induced by superdiffusive spin transport in the Fe junctions is less efficient as that in the Ni-based junctions. Note that the demagnetization values are now plotted for a fluence ten times bigger than in the case of Ni. This is partially understandable because the magnetic moment of Fe (2.2 μ_B/atom) is larger than that of Ni (0.65 μ_B/atom), but a further reduction of the efficiency of the demagnetization has to be ascribed to the reduced asymmetry in the behavior of majority- and minority-spin electrons and the poorer transport properties (velocities and lifetimes) of the hot NEQ electrons in Fe.[65]

What is more interesting is that in both cases of conducting and insulating substrates, the initial demagnetization is followed by a partial recovery. This is ultimately due to the fact that the lifetimes for both spin-majority and spin-minority electrons in Fe are relatively high.[65] To achieve a more precise understanding of the process, we focus on the case of the insulating substrate. After the spatially inhomogeneous excitation by the laser, the diffusion process tends to spread the electronic density evenly. Majority-spin diffusion drives a decrease of magnetization in the more excited regions, whereas minority-spin motion would cause an increase. The mentioned process is more efficient for the spin-majority electrons since they have higher velocities[65] [see the red line in Figs. 7(e1)–7(e3)], but it soon saturates since a completely uniform density is achieved even before the electrons have thermalized (approximate electron thermalization time[46–48] is about 500 fs). Conversely, for spin-minority carriers the process is far less efficient because of the fairly low velocities,[65] but it remains active as long as the electrons have not thermalized [see the blue line in Figs. 7(e1)–7(e3)]. In Fig. 7(f), one may observe how the spin-majority diffusion saturates in less than 100 fs, while the spin-minority diffusion persists until the thermalization is achieved. In the case of the Al substrate the effect reported above is mixed with spin dynamics in Al and the different effects cannot be as easily decoupled.

As the asymmetry of the spin lifetimes and velocities is smaller in Fe than in Ni the superdiffusive spin current injected into the Al layer is different. Spin-minority electrons become more easily trapped at the Fe/Al interface, causing a decrease of Fe magnetization in the interface region. Nonetheless, for Fe more comparable amounts of spin-majority and spin-minority NEQ hot electrons enter the nonmagnetic Al. Consequently, the spin-transfer current induced in the nonmagnetic Al layer has only a net spin polarization of about 65% to maximally 70%, for 100 and 200 fs, respectively.

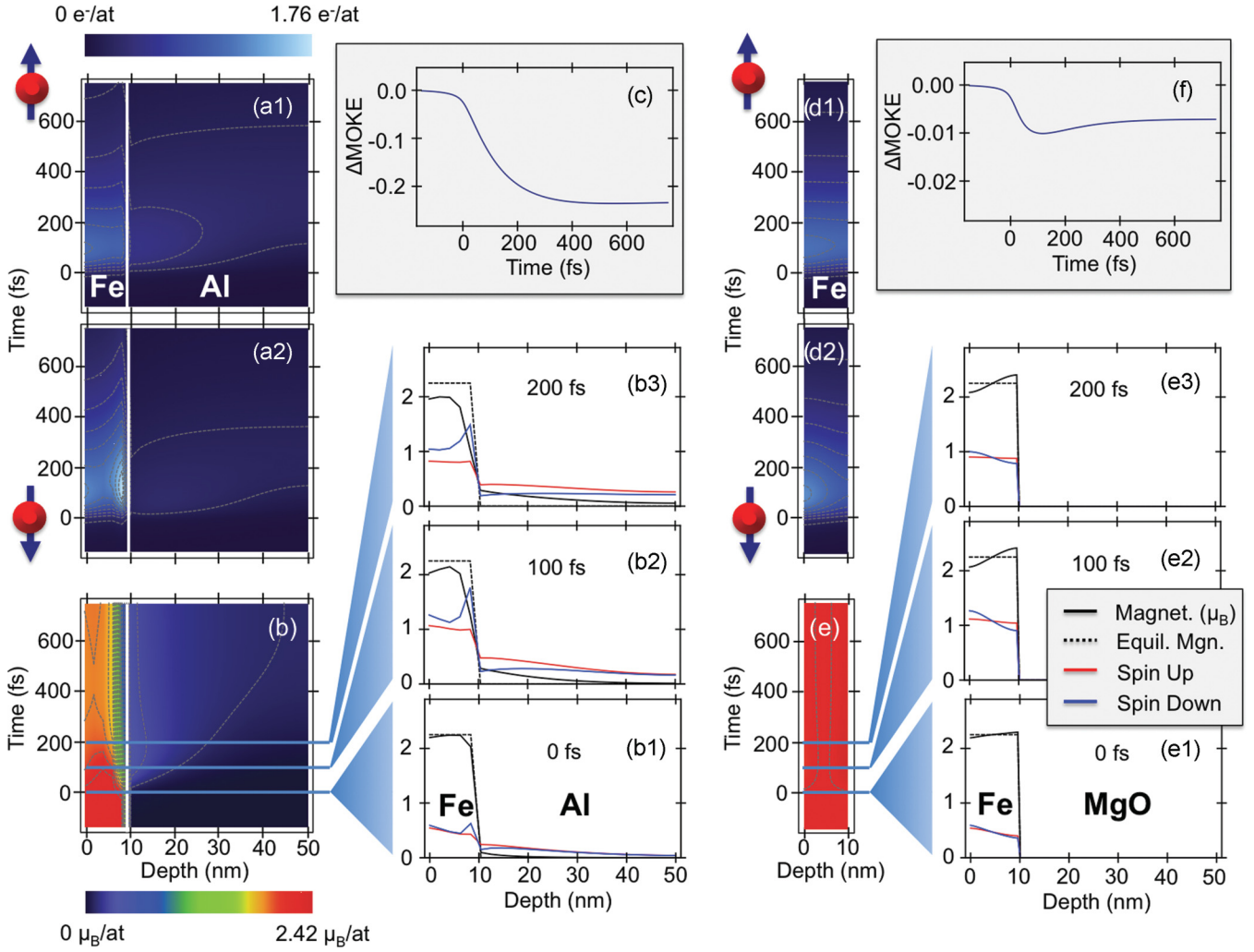

FIG. 7. (Color online) Comparison of ultrafast laser-induced spin dynamics in Fe on different substrates. Panels on the left-hand side show the case of 10 nm of Fe grown on Al, computed for excitation by a laser of 1.5 eV photon-energy and an average number of photons absorbed per Fe atom of 1.0. Panels on the right-hand side display the computed electron and spin dynamics for the case of a 10-nm Fe film grown on an insulating substrate like MgO. The quantities displayed in each panel are the same as given in the caption of Fig. 6.

VIII. DISCUSSION

The above reported investigations reveal several interesting aspects of laser-induced NEQ transport in ferromagnetic/nonmagnetic hybrid junctions. To start with, the obtained results emphasize generally the importance of NEQ spin transport in explanations of ultrafast laser-induced demagnetization. Nearly, all recent theories for ultrafast demagnetization consider an ultrafast, locally operating spin-flip channel,[19,23,24,27,30,36] but completely ignore spin-dependent transport of energetic electrons. Our explicit calculations of laser-induced demagnetization in Ni and Fe hybrid junctions purport that superdiffusive spin transport plays in fact a significant role in achieving an ultrafast spin removal. Moreover, recent *ab initio* investigations[31,35] of how much demagnetization local electron-phonon and electron-electron spin-flip scattering might deliver predicted rather small numbers (a few percent) that are insufficient to explain femtosecond laser-induced demagnetization. Notably, superdiffusive spin transport is highly active as long as the NEQ hot electrons have not thermalized. Electron thermalization times in transition metals are of the order of 500 fs,[46–48] i.e., typically very similar to the time on which the demagnetization process is completed.[17,20,45,66,67,78]

Other model approaches to describe the ultrafast demagnetization, such as the microscopic three temperature model (M3TM)[30] assume an instantaneous thermalization of the excited NEQ electrons, i.e., completed at $t = 0$. Also the Landau-Lifshitz-Bloch and Landau-Lifshitz-Gilbert atomistic approaches[38,40,41] assume the existence of an equilibrated spin-temperature at $t = 0$. Inherent to this assumption is that the effects of NEQ spin transport are excluded in these theoretical approaches. However, an electronic equilibration time of 500 fs would strictly speaking imply that only magnetization dynamics occurring at timescales reasonably larger than 500 fs could reliably be addressed by these model approaches. This would thus be the regime of slower thermal equilibrium magnetization dynamics.

There has recently been an interest in spin currents that can be created in nanodevices, e.g., through spin pumping[50,79,80] or through the spin Seebeck effect.[54,55] An essential difference

between the spin currents created through spin pumping[80] and those induced through femtosecond laser radiation is that the former are *transversal* spin currents whereas the later are *longitudinal* spin currents. Moreover, we anticipate the laser-generated spin currents to be considerably larger than the transversal spin-pumped currents.

Spin currents induced through a temperature gradient in the spin Seebeck effect[54,55] have attracted attention recently; these can for example be employed for spin injection[56] or shifting of magnetic domain walls.[81] We note here that there exists a close analogy between the superdiffusive spin currents and those created in the spin Seebeck effect.[54] The pump laser creates a strong energy concentration gradient in the system by deposing the greatest part of the photons within a region a few times the penetration depth. This happens on a timescale ($\leqslant$500 fs) on which one cannot yet talk about a temperature gradient since the electron system has not yet thermalized. After laser irradiation, the electrons superdiffusively migrate from the "warm" towards the "cold" region due to the excitation inhomogeneity. A first observation of the generation of a thermal spin current due to laser heating and flowing along the temperature gradient was reported recently.[57] In a ferromagnetic material with a strong laser-created energy gradient, the different mobilities of spin-majority and minority electrons favor the superdiffusion of majority-spin carriers resulting in a net longitudinal spin current. In this sense, it would actually not be inappropriate to consider the superdiffusive spin transport as an *ultrafast spin Seebeck effect*. The superdiffusive spin transport is not only an ultrafast counterpart of the spin Seebeck effect, it has the additional advantage of generating longitudinal spin currents that are orders of magnitude larger, yet they act only for a very short time of a few hundred femtoseconds.

IX. CONCLUSION AND OUTLOOK

We have derived a mathematical model to describe the ultrafast diffusion of energetic spin-bearing particles for the case in which the limits of infinitely short lifetimes and mean-free paths and infinitely large velocities—as assumed in the standard thermal diffusion equation—cannot be used. Although the theory may be of general mathematical and physical interest, we have specifically focused on the description of the NEQ charge and spin motion occurring in layered heterostructures after an optical excitation on the femtosecond timescale. Our explicit calculations of the induced superdiffusive particle transport have shown that in ferromagnetic materials it creates a substantial chargeless spin transfer. In particular, in ferromagnetic/nonmagnetic metallic junctions a sizable spin current can be injected in the nonmagnetic layer. Also, we have shown how the superdiffusive spin transfer effect leads to an ultrafast laser-induced demagnetization. The magnitude of the thus-achieved demagnetization is comparable to that observed in femtosecond magneto-optical pump-probe experiments and it can therefore, in principle, completely explain this phenomenon. With the derived model we anticipate to have provided a solid theoretical basis for the emerging area of NEQ femtomagnetotransport.

The generation of ultrafast spin currents in metallic heterostructures through femtosecond laser excitation opens up interesting new avenues for utilization of the spin, rather than the charge, in nanoscale electronic devices. A known obstacle in nanoelectronic devices is the energy loss caused by the flow of the electric current (Joule heating). Employing spin-based transport could considerably reduce the energy dissipation and hence provide a basis for development of energy saving spintronics. Chargeless spin transport has already become considered.[50–53] Extra dimensions that could be added in the near future through laser-generated superdiffusive spin currents are the ultrafast timescale of a few hundreds of femtoseconds of the spin transport as well as the remarkable size of the longitudinal spin-transfer current. Such a large spin current could be employed, for example, to move domain walls in linear magnetic memory devices. Recently, it has predicted that spin currents generated through the spin Seebeck effect could be used for this purpose.[81] This strongly suggests that superdiffusive spin currents—being an ultrafast analog of the spin Seebeck effect—could be utilized for shifting domain walls and even for switching of magnetic nanoelements. More generally, spintronic devices operating on the femtosecond timescale could become realized in the future.

ACKNOWLEDGMENTS

This work has been supported by the Swedish Research Council (VR), by the European Community's Seventh Framework Programme (FP7/2007–2013) under grant agreement No. 214810, "FANTOMAS", and the Swedish National Infrastructure for Computing (SNIC).

*marco.battiato@fysik.uu.se

†Also at Faculty of Mathematics and Physics, Charles University, Ke Karlovu 3, 12116 Prague, Czech Republic.

[1]G. L. Eesley, Phys. Rev. Lett. **51**, 2140 (1983).

[2]H. E. Elsayedali, T. B. Norris, M. A. Pessot, and G. A. Mourou, Phys. Rev. Lett. **58**, 1212 (1987).

[3]R. W. Schoenlein, W. Z. Lin, J. G. Fujimoto, and G. L. Eesley, Phys. Rev. Lett. **58**, 1680 (1987).

[4]S. D. Brorson, J. G. Fujimoto, and E. P. Ippen, Phys. Rev. Lett. **59**, 1962 (1987).

[5]R. Ludeke and A. Bauer, Phys. Rev. Lett. **71**, 1760 (1993).

[6]J. Hohlfeld, J. G. Müller, S. S. Wellershoff, and E. Matthias, Appl. Phys. B **65**, 681 (1997).

[7]M. Bonn, D. N. Denzler, S. Funk, M. Wolf, S. S. Wellershoff, and J. Hohlfeld, Phys. Rev. B **61**, 1101 (2000).

[8]J. Hohlfeld, S. S. Wellershoff, J. Gudde, U. Conrad, V. Jahnke, and E. Matthias, Chem. Phys. **251**, 237 (2000).

[9]R. Knorren, K. H. Bennemann, R. Burgermeister, and M. Aeschlimann, Phys. Rev. B **61**, 9427 (2000).

[10]D. D. Joseph and L. Preziosi, Rev. Mod. Phys. **61**, 41 (1989).

[11]G. Chen, Phys. Rev. Lett. **86**, 2297 (2001).

[12]F. X. Alvarez and D. Jou, Appl. Phys. Lett. **90**, 083109 (2007).

[13]Y.-H. Zhu, B. Hillebrands, and H. C. Schneider, Phys. Rev. B **78**, 054429 (2008).

[14]B. S. Shastry, Rep. Prog. Phys. **72**, 016501 (2009).

[15] Y. Ezzahri and A. Shakouri, Phys. Rev. B **81**, 179901 (2010).
[16] A. Kirilyuk, A. V. Kimel, and T. Rasing, Rev. Mod. Phys. **82**, 2731 (2010).
[17] E. Beaurepaire, J. C. Merle, A. Daunois, and J.-Y. Bigot, Phys. Rev. Lett. **76**, 4250 (1996).
[18] I. Tudosa, C. Stamm, A. B. Kashuba, F. King, H. C. Siegmann, J. Stöhr, G. Ju, B. Lu, and D. Weller, Nature **428**, 831 (2004).
[19] B. Koopmans, J. J. M. Ruigrok, F. Dalla Longa, and W. J. M. de Jonge, Phys. Rev. Lett. **95**, 267207 (2005).
[20] M. Djordjevic, M. Lüttich, P. Moschkau, P. Guderian, T. Kampfrath, R. G. Ulbrich, M. Münzenberg, W. Felsch, and J. S. Moodera, Phys. Status Solidi C **3**, 1347 (2006).
[21] J. Walowski, G. Müller, M. Djordjevic, M. Münzenberg, M. Kläui, C. A. F. Vaz, and J. A. C. Bland, Phys. Rev. Lett. **101**, 237401 (2008).
[22] G. Malinowski, F. Dalla Longa, J. H. H. Rietjens, P. V. Paluskar, R. Huijink, H. J. M. Swagten, and B. Koopmans, Nat. Phys. **4**, 855 (2008).
[23] M. Krauss, T. Roth, S. Alebrand, D. Steil, M. Cinchetti, M. Aeschlimann, and H. C. Schneider, Phys. Rev. B **80**, 180407(R) (2009).
[24] J.-Y. Bigot, M. Vomir, and E. Beaurepaire, Nat. Phys. **5**, 515 (2009).
[25] G. Lefkidis, G. P. Zhang, and W. Hübner, Phys. Rev. Lett. **103**, 217401 (2009).
[26] U. Bovensiepen, Nat. Phys. **5**, 461 (2009).
[27] G. P. Zhang, W. Hübner, G. Lefkidis, Y. Bai, and T. F. George, Nat. Phys. **5**, 499 (2009).
[28] K. Carva, M. Battiato, and P. M. Oppeneer, Nat. Phys. **7**, 665 (2011).
[29] M. Battiato, K. Carva, and P. M. Oppeneer, Phys. Rev. Lett. **105**, 027203 (2010).
[30] B. Koopmans, G. Malinowski, F. Dalla Longa, D. Steiauf, M. Faehnle, T. Roth, M. Cinchetti, and M. Aeschlimann, Nat. Mater. **9**, 259 (2010).
[31] K. Carva, M. Battiato, and P. M. Oppeneer, Phys. Rev. Lett. **107**, 207201 (2011).
[32] A. Melnikov, I. Razdolski, T. O. Wehling, E. T. Papaioannou, V. Roddatis, P. Fumagalli, O. Aktsipetrov, A. I. Lichtenstein, and U. Bovensiepen, Phys. Rev. Lett. **107**, 076601 (2011).
[33] M. Wietstruk, A. Melnikov, C. Stamm, T. Kachel, N. Pontius, M. Sultan, C. Gahl, M. Weinelt, H. A. Duerr, and U. Bovensiepen, Phys. Rev. Lett. **106**, 127401 (2011).
[34] M. Faehnle and C. Illg, J. Phys.: Condens. Matter **23**, 493201 (2011).
[35] S. Essert and H. C. Schneider, Phys. Rev. B **84**, 224405 (2011).
[36] E. Carpene, E. Mancini, C. Dallera, M. Brenna, E. Puppin, and S. De Silvestri, Phys. Rev. B **78**, 174422 (2008).
[37] M. Djordjevic and M. Münzenberg, Phys. Rev. B **75**, 012404 (2007).
[38] U. Atxitia, O. Chubykalo-Fesenko, N. Kazantseva, D. Hinzke, U. Nowak, and R. W. Chantrell, Appl. Phys. Lett. **91**, 232507 (2007).
[39] U. Atxitia, O. Chubykalo-Fesenko, J. Walowski, A. Mann, and M. Münzenberg, Phys. Rev. B **81**, 174401 (2010).
[40] U. Atxitia and O. Chubykalo-Fesenko, Phys. Rev. B **84**, 144414 (2011).
[41] T. A. Ostler *et al.*, Nat. Commun. **3**, 666 (2012).
[42] K. Vahaplar *et al.*, Phys. Rev. B **85**, 104402 (2012).
[43] G. M. Müller *et al.*, Nat. Mater. **8**, 56 (2009).
[44] L. M. Sandratskii and P. Mavropoulos, Phys. Rev. B **83**, 174408 (2011).
[45] S. Mathias *et al.*, Proc. Natl. Acad. Sci. USA **109**, 4792 (2012).
[46] C.-K. Sun, F. Vallée, L. Acioli, E. P. Ippen, and J. G. Fujimoto, Phys. Rev. B **48**, 12365 (1993).
[47] C. Guo, G. Rodriguez, and A. J. Taylor, Phys. Rev. Lett. **86**, 1638 (2001).
[48] H.-S. Rhie, H. A. Dürr, and W. Eberhardt, Phys. Rev. Lett. **90**, 247201 (2003).
[49] M. Lisowski, P. A. Loukakos, U. Bovensiepen, J. Stähler, C. Gahl, and M. Wolf, Appl. Phys. A **78**, 165 (2004).
[50] Y. Tserkovnyak, A. Brataas, and G. E. W. Bauer, Phys. Rev. Lett. **88**, 117601 (2002).
[51] E. Simanek and B. Heinrich, Phys. Rev. B **67**, 144418 (2003).
[52] M. V. Costache, M. Sladkov, S. M. Watts, C. H. van der Wal, and B. J. van Wees, Phys. Rev. Lett. **97**, 216603 (2006).
[53] G. Woltersdorf, O. Mosendz, B. Heinrich, and C. H. Back, Phys. Rev. Lett. **99**, 246603 (2007).
[54] K. Uchida, S. Takahashi, K. Harii, J. Ieda, W. Koshibae, K. Ando, S. Maekawa, and E. Saitoh, Nature **455**, 778 (2008).
[55] C. M. Jaworski, J. Yang, S. Mack, D. D. Awschalom, J. P. Heremans, and R. C. Myers, Nat. Mater. **9**, 898 (2010).
[56] A. Slachter, F. L. Bakker, J.-P. Adam, and B. J. van Wees, Nat. Phys. **6**, 879 (2010).
[57] M. Weiler *et al.*, Phys. Rev. Lett. **108**, 106602 (2012).
[58] P. M. Oppeneer and A. Liebsch, J. Phys.: Condens. Matter **16**, 5519 (2004).
[59] B. Koopmans, M. van Kampen, and W. J. M. de Jonge, J. Phys.: Condens. Matter **15**, S723 (2003).
[60] F. Dalla Longa, J. T. Kohlhepp, W. J. M. de Jonge, and B. Koopmans, Phys. Rev. B **75**, 224431 (2007).
[61] L. Braicovich and G. van der Laan, Phys. Rev. B **78**, 174421 (2008).
[62] J. P. Bouchaud and A. Georges, Phys. Rep. **195**, 127 (1990).
[63] R. Metzler and J. Klafter, Phys. Rep. **339**, 1 (2000).
[64] R. Knorren, G. Bouzerar, and K. H. Bennemann, J. Phys.: Condens. Matter **14**, R739 (2002).
[65] V. P. Zhukov, E. V. Chulkov, and P. M. Echenique, Phys. Rev. B **73**, 125105 (2006).
[66] B. Koopmans, M. van Kampen, J. Kohlhepp, and W. de Jonge, Phys. Rev. Lett. **85**, 844 (2000).
[67] C. Stamm *et al.*, Nat. Mater. **6**, 740 (2007).
[68] C. Stamm, N. Pontius, T. Kachel, M. Wietstruk, and H. A. Dürr, Phys. Rev. B **81**, 104425 (2010).
[69] G. Grosso and G. Pastori Parravicini, *Solid State Physics* (Academic Press, London, 2000), Chap. VII.
[70] A. Chasse, H. A. Dürr, G. van der Laan, Y. Kucherenko, and A. N. Yaresko, Phys. Rev. B **68**, 214402 (2003).
[71] R. Ludeke and A. Bauer, Phys. Rev. Lett. **71**, 1760 (1993).
[72] V. P. Zhukov, E. V. Chulkov, and P. M. Echenique, Phys. Rev. B **72**, 155109 (2005).
[73] A. Grechnev, I. Di Marco, M. I. Katsnelson, A. I. Lichtenstein, J. Wills, and O. Eriksson, Phys. Rev. B **76**, 035107 (2007).
[74] E. Beaurepaire, M. Maret, V. Halte, J. C. Merle, A. Daunois, and J.-Y. Bigot, Phys. Rev. B **58**, 12134 (1998).
[75] D. Cheskis, A. Porat, L. Szapiro, O. Potashnik, and S. Bar-Ad, Phys. Rev. B **72**, 014437 (2005).

[76] A. Quarteroni, R. Sacco, and F. Saleri, *Numerical Mathematics* (Springer, Berlin, 2007).
[77] K. Carva, D. Legut, and P. M. Oppeneer, Europhys. Lett. **86**, 57002 (2009).
[78] T. Kampfrath, R. G. Ulbrich, F. Leuenberger, M. Münzenberg, B. Sass, and W. Felsch, Phys. Rev. B **65**, 104429 (2002).
[79] Y. Tserkovnyak, A. Brataas, and G. E. W. Bauer, Phys. Rev. B **66**, 224403 (2002).
[80] Y. Tserkovnyak, A. Brataas, G. E. W. Bauer, and B. I. Halperin, Rev. Mod. Phys. **77**, 1375 (2005).
[81] D. Hinzke and U. Nowak, Phys. Rev. Lett. **107**, 027205 (2011).